**Supporting Information**

# Synergistic effect between 1D $Co_3S_4/MoS_2$ heterostructures to boost the performance for alkaline overall water splitting

*Zilong Li [a], Weilong Xu [a], Xiaolong Yu [b], Sanxi Yang [a], Yang Zhou *, [a], Kai Zhou [c], Qikai, Wu [d], Shunlian Ning [d], Mi Luo [d], Dengke Zhao *, [d] and Nan Wang *, [a]*

Z. L. Li, W.L. Xu, S. X. Yang, Y. Zhou, and N. Wang
College of Science and Engineering, Jinan University, Guangzhou 510632, China
E-mail: nanwang@jnu.edu.cn

X. L. Yu
Guangdong Provincial Key Laboratory of Petrochemical Pollution Processes and Control, School of Environmental Science and Engineering, Guangdong University of Petrochemical Technology, Maoming, Guangdong 525000, China

K. Zhou
Center for Advanced Analytical Science, c/o School of Chemistry and Chemical Engineering Guangzhou University Guangzhou 510006, P.R. China.

Q. K. Wu, S. L. Ning, M. Luo and D. K. Zhao
New Energy Research Institute, College of Environment and Energy, South China University of Technology, Guangzhou 510006, China

* The Corresponding authors:
E-mail: yangzhou@email.jnu.edu.cn (Yang Zhou), scutezhao@sina.com (Dekeng Zhao), nanwang@jnu.edu.cn (Nan Wang)

**List of Contents**

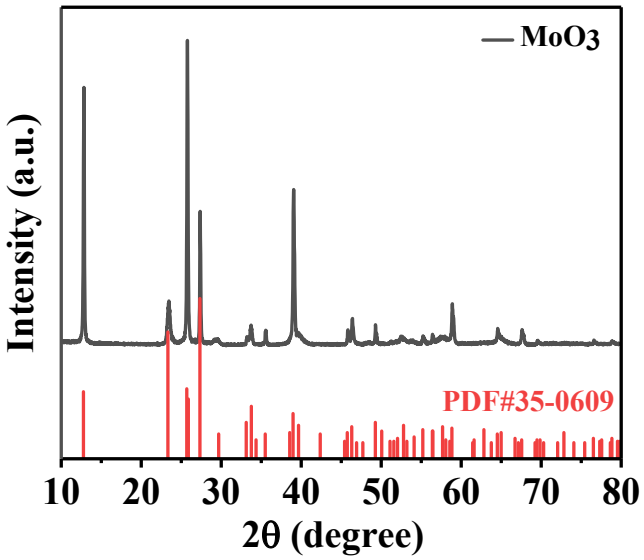


**Figure S1.** XRD pattern of $MoO_3$.

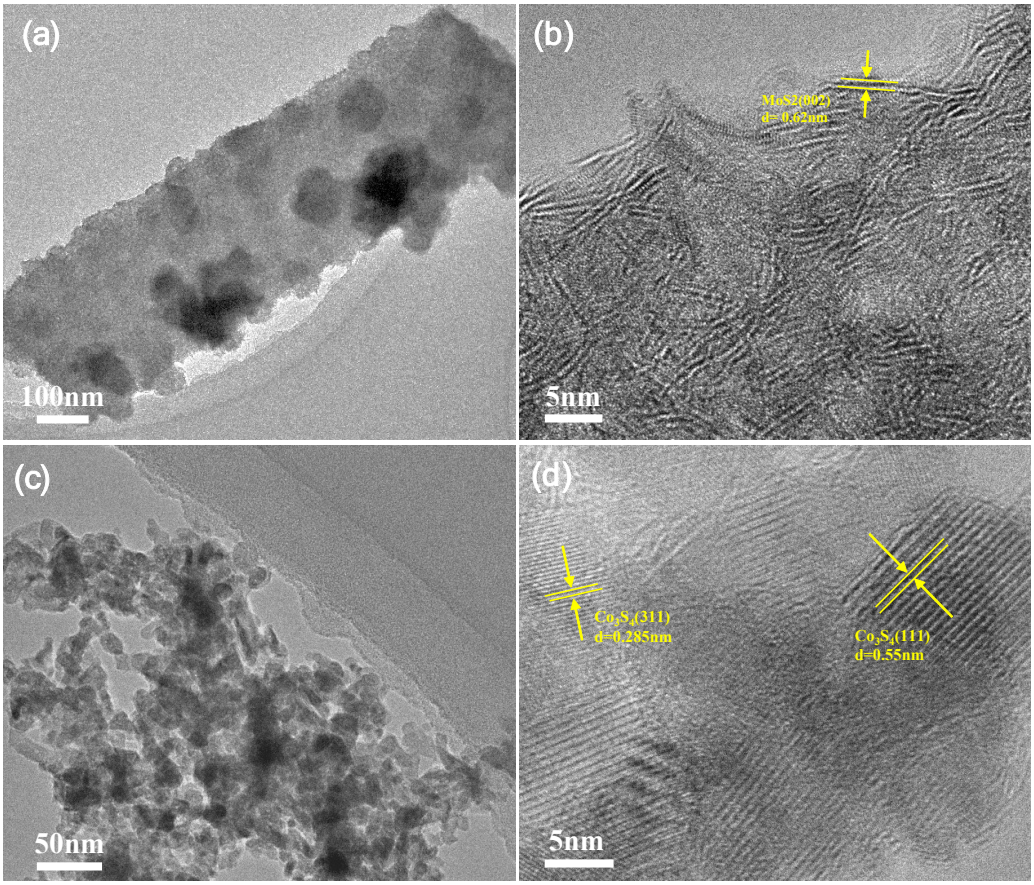


**Figure S2.** (a, c) TEM images of $MoS_2$ NR and $Co_3S_4$. (b, d) the corresponding HRTEM images of $MoS_2$ NR and $Co_3S_4$.

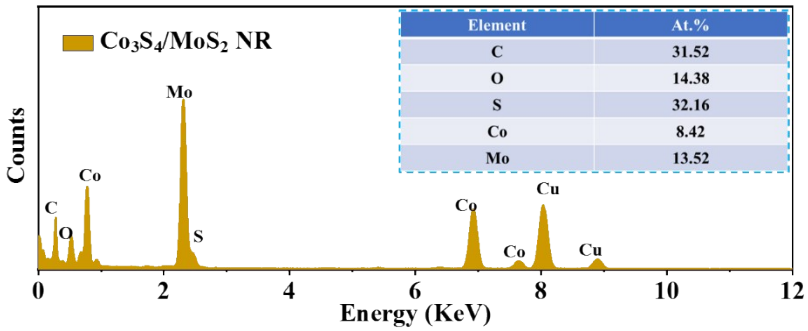


**Figure S3**. The TEM-EDS spectrum of $Co_3S_4/MoS_2$ NR.

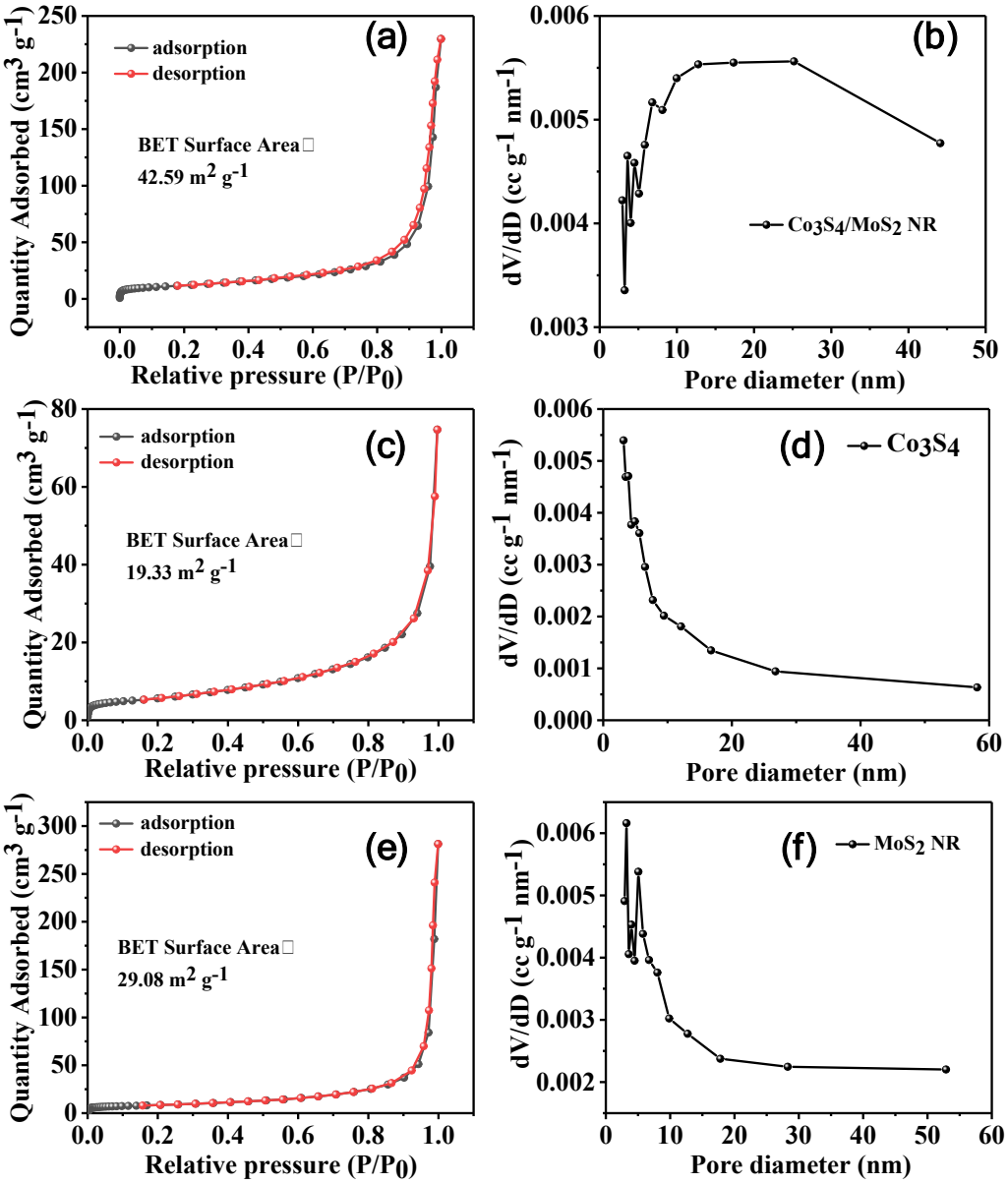


**Figure S4. (a, c, e)** Nitrogen adsorption-desorption isotherms of as-made samples. (b, d, f) the corresponding pore-size distribution plots of as-made samples.

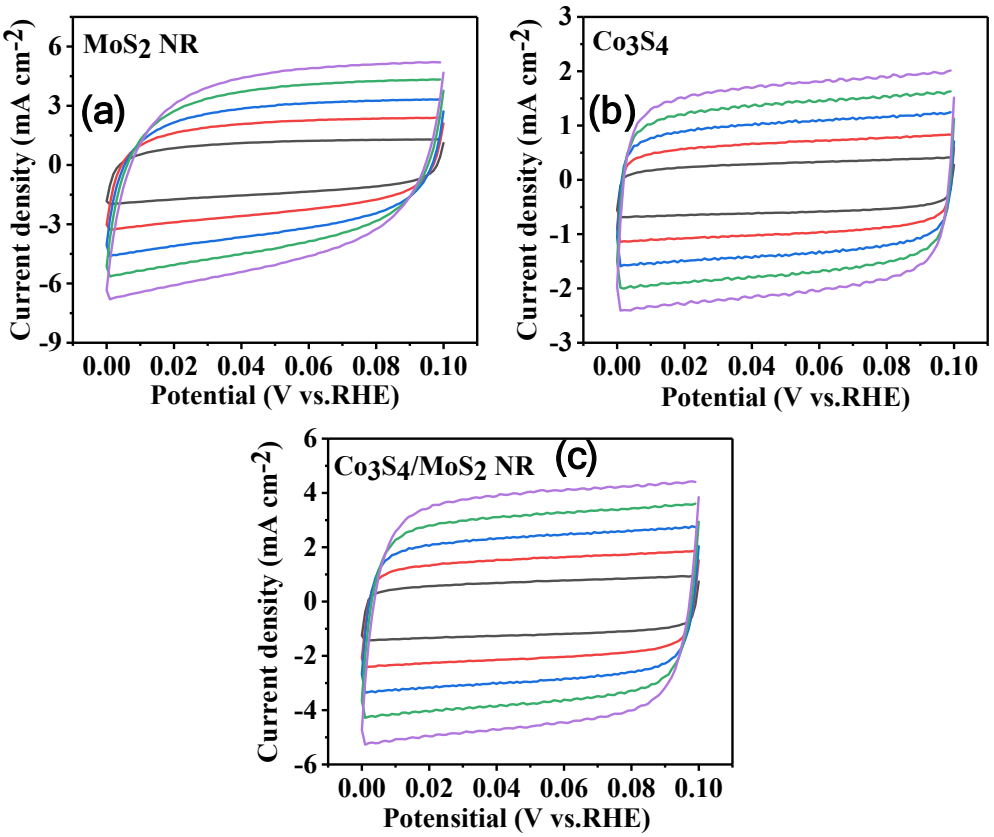


**Figure S5.** (a, b, c) CV measurements with different scan rates (40, 80, 120, 160 and 200 mV $s^{-1}$) at different potential ranges (0.00-0.10 V vs. RHE) in 1 M KOH solution.

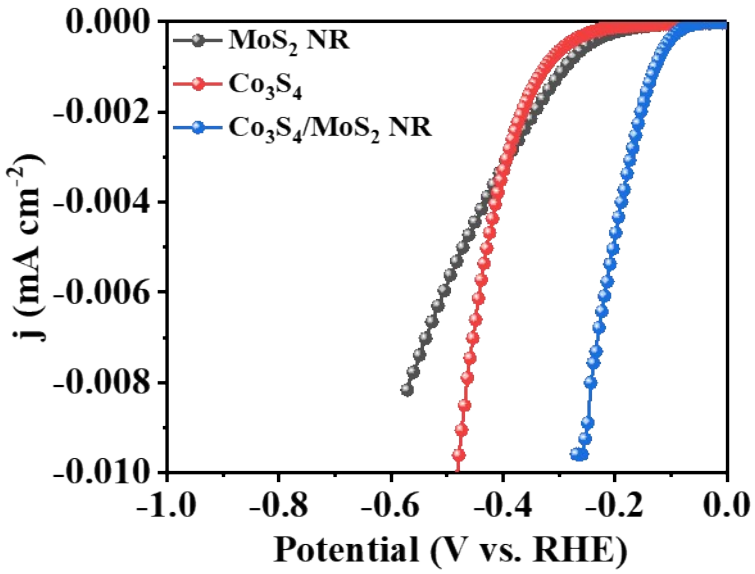


**Figure S6.** The LSV normalized by ECSA of different samples

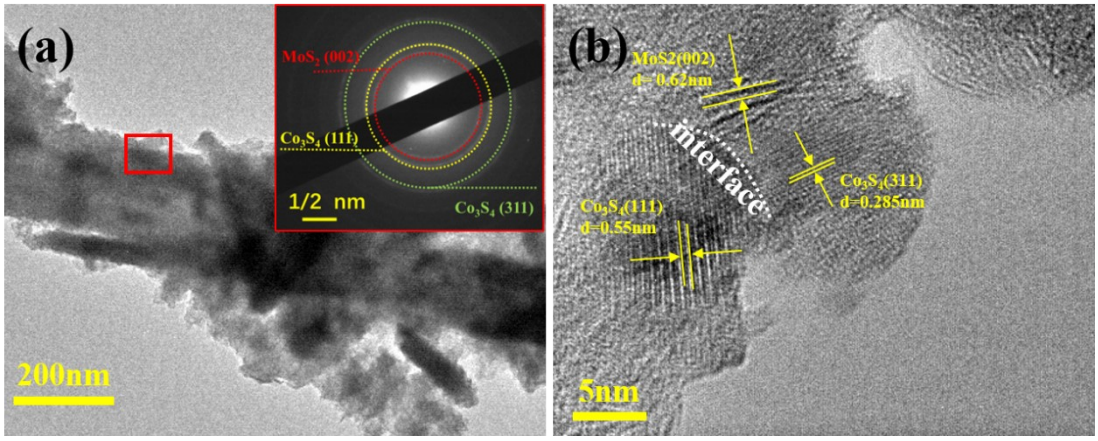


**Figure S7.** (a, b) The TEM and HRTEM images of $Co_3S_4/MoS_2$ NR after long-time HER test.

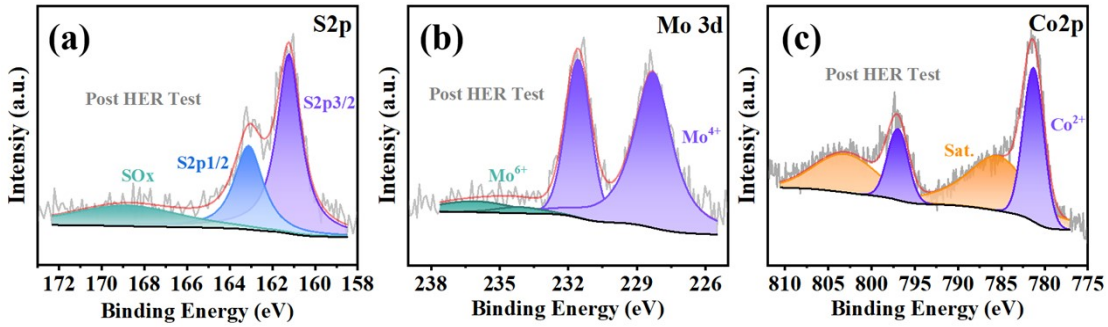


**Figure S8.** (a, b, c) The S 2p, Mo 3d and Co 2p of $Co_3S_4/MoS_2$ NR after long-time HER test.

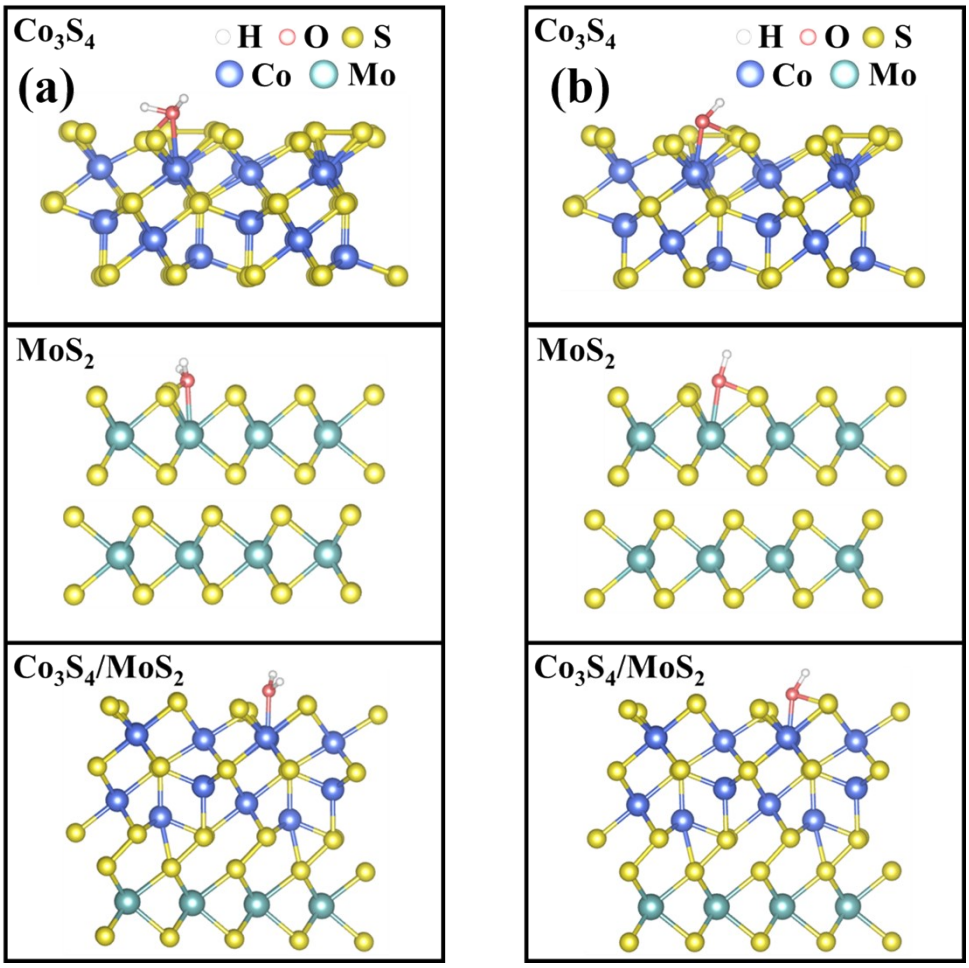


**Figure S9.** Scheme of $Co_3S_4$ (111), $MoS_2$ (002) and $Co_3S_4/MoS_2$ heterostructure with $H_2O$ (a) and OH (b) adsorbed on the respective surface.

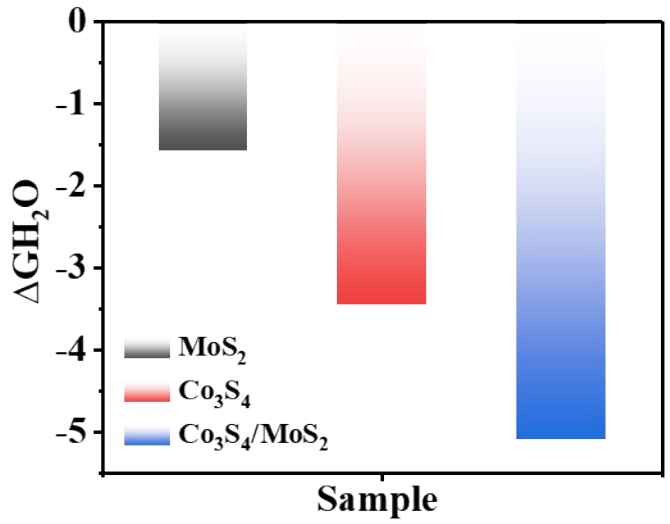


**Figure S10.** DFT-calculated $H_2O$ free-energy change of $Co_3S_4$ (111), $MoS_2$ (002) and $Co_3S_4/CoS_2$ heterostructure.

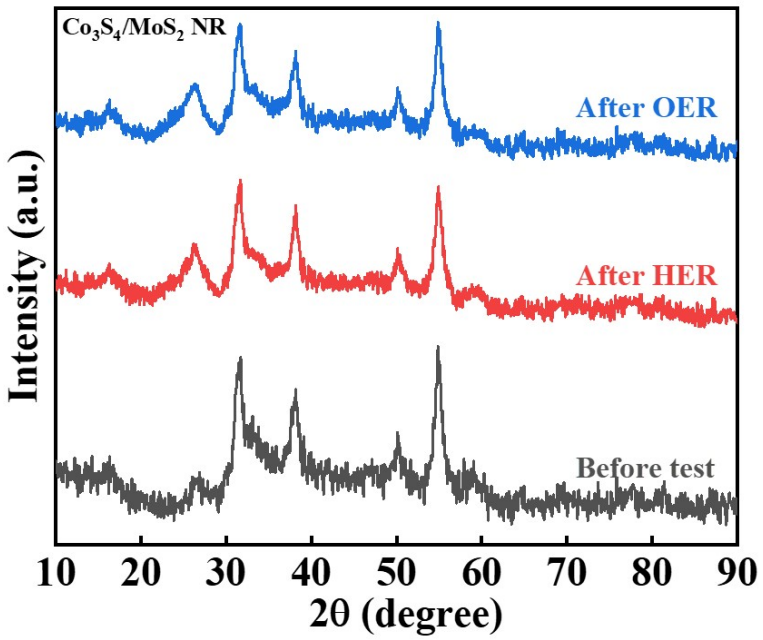


**Figure S11.** XRD pattern of $Co_3S_4/MoS_2$ NR before and after HER and OER test.

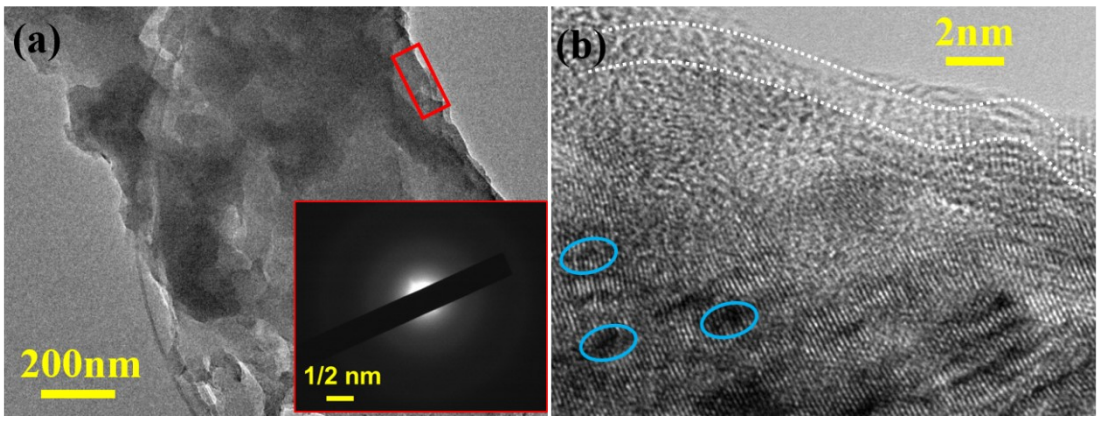


**Figure S12.** (a, b) The TEM and HRTEM images of $Co_3S_4/MoS_2$ NR after long-time OER test.

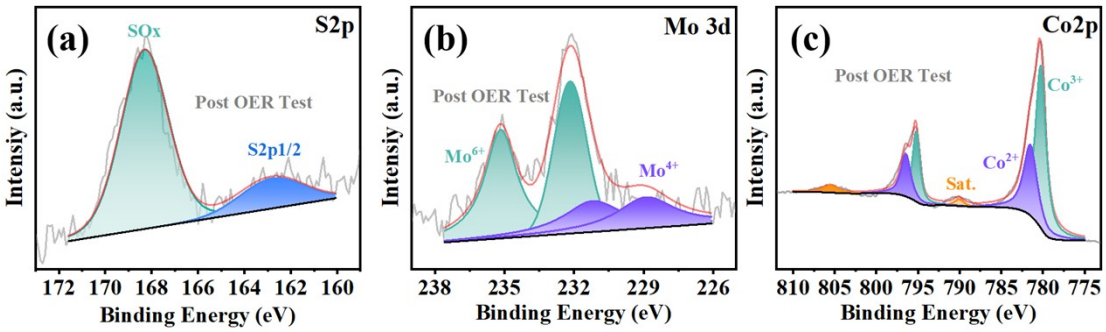


**Figure S13.** (a, b, c) The S 2p, Mo 3d and Co 2p of $Co_3S_4/MoS_2$ NR after long-time OER test.

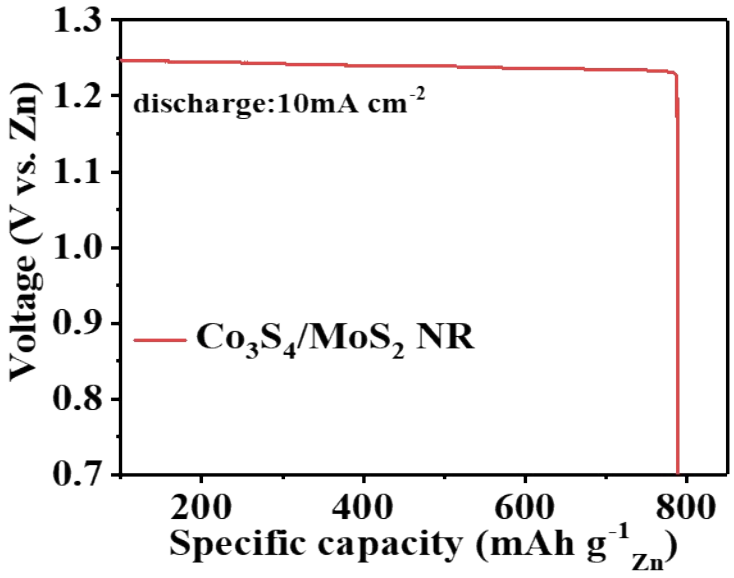


**Figure S14.** The galvanostatic discharge curves of a r-ZAB loaded with $Co_3S_4/MoS_2$ NR catalysts on air cathode

**Table S1.** Comparison of the electrochemical HER and OER performance of $Co_3S_4/MoS_2$ NR with some leading non-precious bifunctional electrocatalysts.

| Electrocatalyst | Catalytic performance | | Reference information |
|---|---|---|---|
| | Overpotential ($j_{10}$) of HER (mV) | Overpotential ($j_{10}$) of OER (mV) | |
| **$Co_3S_4/MoS_2$ NR** | **116** | **280** | **This work** |
| Co@Co-P@NPCNTs | 160 | 290 | Ref.44 (2020) |
| FeOOH/$Ni_3N$ | 67 | 244 | Ref.45 (2020) |
| $Co_4N$@NC | 62 | 257 | Ref.46 (2020) |
| VOOH-3Fe | 90 | 195 | Ref.47 (2020) |
| CoFeO@BP | 88 | 266 | Ref.48 (2020) |
| Co/CoP@HOMC | 120 | 260 | Ref.49 (2021) |
| WN-Ni@N,P-CNT | 70 | 268 | Ref.50 (2021) |
| Ni-Mo-P | 69 | 235 | Ref.51 (2021) |
| $MoS_2$/NiFe-LDH | 110 | 210 | Ref.52 (2019) |
| Co-$Ni_3N$ | 194 | 307 | Ref.53 (2018) |
| NiFe-MOF-5 | 163 | 168 | Ref.54 (2021) |
| $Co_9S_8$@$Co_9S_8$@$MoS_{2-x}$ | 173 | 340 | Ref.55 (2019) |
| Co@N-CNTF | 220 | 350 | Ref.56 (2019) |
| $FeS_2$@MXene | 87 | 240 | Ref.57 (2022) |
| Ni-Co sulfide/NF | 190 | 230 | Ref.58 (2021) |